

Spin-dependent electronic and magnetic properties of Co nanostructures on Pt(111) studied by spin-resolved scanning tunneling spectroscopy

F. Meier,* K. von Bergmann, P. Ferriani, J. Wiebe, M. Bode, K. Hashimoto, S. Heinze, and R. Wiesendanger
Institute of Applied Physics, University of Hamburg, Jungiusstraße 11, 20355 Hamburg, Germany

(Received 23 June 2006; revised manuscript received 11 September 2006; published 13 November 2006)

Spin-resolved scanning tunneling spectroscopy measurements at low temperatures were performed for Co nanostructures on Pt(111). On Co monolayer islands and wires the electronic structure changes on the scale of a few atoms due to the changing local stacking of the Co atoms. First-principles calculations for pseudomorphic fcc and hcp stacked Co monolayers assign the dominant feature in the measured spectra to a d -like surface resonance of minority-spin character which shifts in energy because of a different coupling to the Pt substrate. Despite the heterogeneous electronic structure of the Co monolayer, the out-of-plane magnetized domains are clearly observed. While the domain wall width measured on wires is less than 4 nm there is no indication for a change in the magnetization direction for islands with a base length up to fifteen times the domain wall width. Furthermore, the magnetic hysteresis in an ensemble of out-of-plane magnetized Co monolayer as well as double-layer nanostructures was observed. While the coercivity for the monolayer nanostructures is about 0.25 T, double-layer islands show surprisingly large coercivities of more than 2 T.

DOI: [10.1103/PhysRevB.74.195411](https://doi.org/10.1103/PhysRevB.74.195411)

PACS number(s): 68.37.Ef, 75.75.+a, 71.15.Mb, 73.20.At

I. INTRODUCTION

Cobalt nanostructures on noble metal substrates provide interesting model systems to study magnetic properties in reduced dimensions.¹⁻⁷ In particular the system Co/Pt(111) has received great attention due to its potential application in magnetic recording media. Recently a number of experimental reports have demonstrated the significant interest in the exciting magnetic properties of low-dimensional Co structures on Pt(111): Gambardella *et al.* showed how magnetic properties like coercivity and anisotropy can be changed for low dimensional Co structures like single atoms and wires.^{1,2} The experiments on single Co atoms located on Pt(111) terraces reveal a giant magnetic out-of-plane anisotropy while the magnetic orientation of ferromagnetic Co wires decorating Pt step edges is canted with respect to the surface normal.^{1,2} Furthermore, an increase of the width of the Co wires leads to significant changes of the anisotropy direction and the coercivities.⁸ Measurements performed on nanoscale monolayer (ML) high Co islands on Pt(111) by Rusponi *et al.* reveal an out-of-plane anisotropy of these structures which is stabilized to a large extent by the perimeter atoms.³ These interesting results strikingly demonstrate that the magnetic properties of structures in the nanometer range cannot be rationalized without taking into account the dimensionality, size, shape, environment, and interface structure. While most of the experimental results concerning the magnetic properties of Co/Pt(111) samples were obtained by spatially averaging methods based on the magneto-optical Kerr effect (MOKE) and x-ray magnetic circular dichroism (XMCD), there is only one recent spin-sensitive scanning tunneling microscopy (STM) study which was able to distinguish double-layer islands with opposite out-of-plane magnetization orientations.⁹

However, Co monolayer and double layers on Pt(111) have already proven to be complicated systems on the atomic scale. A detailed insight into the growth and the structural properties of ultrathin Co films on Pt(111) has been obtained

by STM experiments at room temperature.^{10,11} Lundgren *et al.* (Ref. 11) studied the dislocation network of the Co monolayer on Pt(111), which is formed due to the lattice mismatch of 9.4% between Pt and Co. They observed that the Co atoms preferentially occupy fcc sites while a much smaller number of Co atoms was found on hcp sites. To relieve the strain structural domain walls are introduced consisting of Co atoms in bridge site positions. These results indicate a spatially inhomogeneous electronic structure, which has direct impact on the magnetic properties of this system.

These former STM experiments did not include electronic structure measurements, and we are not aware of such a study performed for Co ultrathin films on Pt(111). Only one recent scanning tunneling spectroscopy (STS) study on single Co atoms on Pt(111) showed a spectroscopic difference of Co atoms occupying different stacking sites.¹² Also investigations of Co nanostructures on other substrates have shown some interesting properties which may be of importance for the sample system Co/Pt(111) being the focus of this work. For instance experiments revealing the electronic structure of Co nanostructures and films were performed on Co islands on Cu(111),^{4,5,13} on Co/Cu/Co sandwiches,¹⁴ and on ultrathin as well as thick Co films on W(110)¹⁵⁻¹⁷ by STS. For Co islands on Cu(111) and Co films on W(110) it was possible to distinguish islands and more extended areas of different stacking spectroscopically.^{5,13,15,17} In addition, by performing first-principles electronic structure calculations, Wiebe *et al.*¹⁷ showed that this observation can be explained by a different coupling strength of the Co surface resonance to the bulk states. This surface resonance showed up as a dominant peak in the differential conductance spectra below the Fermi energy E_F at about -0.3 eV.^{4,5,14,17} Apart from the correlation between structural and electronic properties Pietzsch *et al.*⁵ probed the magnetic state of the Co islands by spin-resolved STS. Besides a large energy-dependent spin-polarization they found a perpendicular magnetization of the Co islands and a coercivity between 1.0–1.5 T by measuring in the presence of variable external magnetic fields.

To gain further insight into the interplay between structural, electronic, and magnetic properties of Co nanostructures on Pt(111) we performed an extensive study on monolayer Co islands and wires. In addition we studied the magnetic properties of Co double-layer islands on Pt(111). We applied the experimental method of spin-polarized (SP)-STM, which combines a very high lateral resolution with magnetic sensitivity and gives access to the local electronic structure.¹⁸

This paper is organized as follows: Sec. II gives a brief introduction into the experimental setup, tip and sample preparation, and measurement procedures. In Sec. III A the spatially resolved electronic structure of oppositely magnetized Co monolayer islands and wires and its correlation to the local stacking is shown. These measurements are compared to first-principles calculations of extended pseudomorphic hcp and fcc Co monolayer films on Pt(111). In Sec. III B we discuss the response of Co monolayer and double-layer nanostructures to an external magnetic field.

II. EXPERIMENTAL DETAILS

All experiments were performed in a multichamber ultra-high vacuum system.²⁰ It contains a home-built scanning tunneling microscope operating with the tip and sample held at $T=13\pm 1$ K and several standard devices for preparation and analysis of samples and tips. Using a superconducting split-coil magnet a maximum magnetic field B of 2.5 T perpendicular to the sample surface is available. The base pressure of the system is in the low 10^{-11} mbar range.

All topographic STM images were recorded in the constant-current mode. In this mode the stabilization current I_{stab} is kept constant with closed feedback while applying a fixed bias voltage U to the sample. To obtain information about the electronic structure of the sample the differential conductance $dI/dU(U)$ signal is measured, which is closely related to the local density of states (LDOS) of the sample at the corresponding energy eU .²¹ In order to perform such spectroscopy measurements the tip is first stabilized at U_{stab} and I_{stab} . Then the feedback is deactivated, the voltage is swept to a final value, and $I(U)$ as well as $dI/dU(U)$ are recorded. The $dI/dU(U)$ spectra are obtained by using a lock-in technique where a small *ac* modulation voltage U_{mod} is added to U ($f=3.0-4.0$ kHz, $U_{\text{mod}}=20$ mV). This can be done for each image point thus achieving $dI/dU(U)$ spectra with high lateral resolution, or so-called full spectroscopy fields. A less time-consuming method to get access to the electronic properties of the sample is the measurement of so-called dI/dU maps at a fixed bias voltage. In contrast to dI/dU spectra, dI/dU maps are obtained by recording the dI/dU signal simultaneously to constant-current images with a closed feedback loop. In the following the spatially resolved dI/dU signal at a fixed bias voltage extracted from a full spectroscopy field is called a dI/dU slice in order to distinguish it from a dI/dU map.

The Pt(111) surface was prepared by cycles of Ar⁺-ion sputtering at room temperature and subsequent annealing at 1500 K for 4 min. Occasionally, an additional annealing at 1000 K in an oxygen atmosphere of 3×10^{-7} mbar was car-

ried out for 20 min. For monolayer high nanostructures Co was deposited on the clean Pt(111) surface from a rod in a water-cooled e-beam evaporator at room temperature. A typical deposition rate was 0.4 atomic layers (AL) per minute. We define a coverage of one AL as a complete coverage of the Pt substrate with Co atoms. To obtain double-layer Co islands, the Pt crystal was precooled in the microscope to 13 K and then transferred to the evaporation stage. After Co deposition the sample was slightly annealed to approximately 340 K which results in double-layer Co islands on the Pt surface as described in the literature.³

All STM tips were etched electrochemically from polycrystalline tungsten wire and flashed *in vacuo* to 2000 K. For the spin-resolved measurements the tips were afterwards coated with thin films of antiferromagnetic (Cr) or ferromagnetic (Fe) materials.²² The use of magnetic tips allows the measurement of the spin-resolved dI/dU signal, which depends on the scalar product of tip and sample magnetization.²² Thereby any differences in spin-resolved dI/dU signals observed for structures exhibiting the same spin-averaged electronic structure are due to a different relative alignment of the tip and sample magnetization vectors. In the following the appearance of these differences in spin-resolved dI/dU maps is called magnetic contrast. Since monolayer and double-layer high Co islands on Pt(111) are known to exhibit an out-of-plane magnetization³ the largest magnetic contrast is expected for tips with a magnetization pointing perpendicular to the surface. It is known that Cr-coated tips with a coverage below 40 AL are sensitive to the out-of-plane component of the sample magnetization.²³ In this study the Cr coverage was 15–20 AL. While Fe-coated tips are usually magnetized in the surface plane, sometimes they also show an out-of-plane component of the magnetization. Using Fe-coated tips (10–15 AL) can be advantageous due to a higher spin polarization of the electronic states compared to Cr-coated tips. This can lead to a higher magnetic contrast in dI/dU maps even though the tip magnetization is mainly in plane. A possible explanation for an Fe tip with a larger out of plane component, i.e., an unusual anisotropy direction, is the adhesion of sample material after voltage pulses which are used in order to sharpen the tip.

III. RESULTS

A. Structure and spin-resolved electronic properties of the Co monolayer

1. Experimental results

Figure 1(a) shows a topographic image of 0.3 AL Co deposited on Pt(111) at room temperature. On the terrace one atomic layer high Co islands are observed coexisting with one atomic layer high Co wires at the step edges. The Co islands are triangularly shaped with a base length from 60 nm down to a few nm. All islands point in the same direction and some larger ones already show the nucleation of the second atomic layer on top. The faint lines visible on the Pt substrate which are indicated by the arrows can be identified as Co induced double row reconstruction lines.^{10,24} The inset shows the area marked by the white rectangle at a

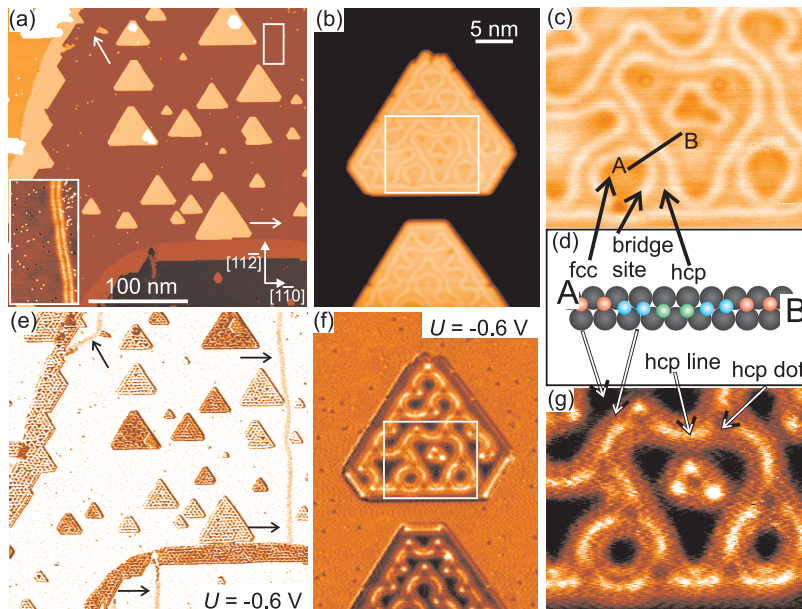


FIG. 1. (Color online) Co monolayer islands and wires prepared by Co deposition on the Pt(111) surface at room temperature. Upper panels (a)–(c): Topographic images. Inset in (a): Magnified view of the Co induced double row reconstruction lines. (d) Sketch of the different stacking along the line drawn in (c) (Ref. 19). Lower panels (e)–(g): dI/dU maps measured simultaneously to the topographic images of the upper panel with out-of-plane sensitive magnetic tips.

closer view and displays the characteristic two parallel bright lines on the Pt substrate. The existence of this kind of reconstruction is indicative of the incorporation of Co atoms into the topmost Pt layer.²⁴ Since it is known that the double row reconstruction lines run along $\langle 11\bar{2} \rangle$, i.e., perpendicular to closed-packed rows, we can conclude that all edges of the Co islands as well as of the Co wires are parallel to the closed-packed rows. Furthermore, it can be observed that the roughness of the Co wires is smaller when the Pt step edge runs along a closed-packed row, as seen in the bottom right part of Fig. 1(a).

Figure 1(b) shows two slightly truncated triangular shaped Co islands. Both exhibit a mostly voltage independent narrow dislocation network on top which is always found for Co monolayer islands as well as wires. Figure 1(c) displays a magnified view of the area marked by the box in (b) and reveals that the network is formed by brighter lines with a relative height of about 10 pm. The same network has been found in a previous STM study on Co monolayer films on Pt(111).¹¹ It is due to inhomogeneous stacking of the Co atoms caused by the strain of the overlayer. This strain is induced by the mismatch of -9.4% between the Co and the Pt lattice and relieved by the formation of dislocation lines. According to Ref. 11 the Co atoms preferentially occupy the fcc sites of the Pt lattice. The dislocation lines appear slightly higher and are formed by Co atoms taking bridgesites separating fcc and hcp stacked regions. Taking these results into account we can assign the more extended areas visible in Fig. 1(c) to fcc areas while the brighter lines are formed by Co atoms occupying bridgesites. Furthermore, the narrow areas in between the lines consist of Co atoms in hcp positions of the Pt lattice. Figure 1(d) sketches the local stacking of the Co atoms below the line drawn in (c) which connects two fcc regions while passing two bridgesite lines and one narrow hcp area. The smallest distance between two bridgesite lines is about $8 \pm 1 \text{ \AA}$, which leads to very narrow hcp regions of only a couple of atoms (Pt nearest neighbor distance is 2.77 \AA).

Figure 1(e) shows an out-of-plane sensitive magnetic dI/dU map recorded simultaneously to Fig. 1(a). The Pt surface appears homogeneous except above the Co induced double row reconstruction lines indicated by the arrows. Above the Co wires and islands a dominating two color contrast in the dI/dU signal is found. Since all Co wires as well as all islands have an identical spin-averaged electronic structure we ascribe the origin of this contrast to oppositely magnetized domains of the Co monolayer. We conclude that the Co monolayer has an easy axis normal to the surface plane in agreement with former results obtained by spatially averaging methods for Co on Pt(111) in the submonolayer regime.^{3,8,25} This will be proven in Sec. III B. The relative magnetization direction of the Co nanostructures can easily be deduced from the dominant colors of the wires and single domain islands. In addition to the magnetic contrast the appearance of the dI/dU signal above the nanostructures appears highly heterogeneous. A comparison of the dI/dU map of two oppositely magnetized single domain islands in (f) to the simultaneously recorded topographic image (b) reveals that these small scale variations of the dI/dU signal are directly correlated to the reconstruction due to the strain relief. In order to investigate this correlation in more detail Fig. 1(g) shows a magnified view of the region marked in (f). By comparing this dI/dU map (g) to the corresponding topography in (c) each dI/dU level can directly be assigned to the local stacking of the atoms: while fcc and hcp areas show the same height in topography, both stackings show different dI/dU intensities and can easily be distinguished. At the applied bias voltage of -0.6 V the highest dI/dU intensity is obtained for the hcp-lines followed by the signal above the bridgesite lines while the fcc areas show the lowest intensity. Interestingly, we can identify a fourth distinct area in dI/dU which has not been seen in the topography. This fourth distinct area is located at positions where three hcp-lines come together and will be called hcp-dot in the following. By comparing the two oppositely magnetized islands in Fig. 1(f) it becomes obvious that the four stackings are also observed for the lower island. However, due to the different magnetic

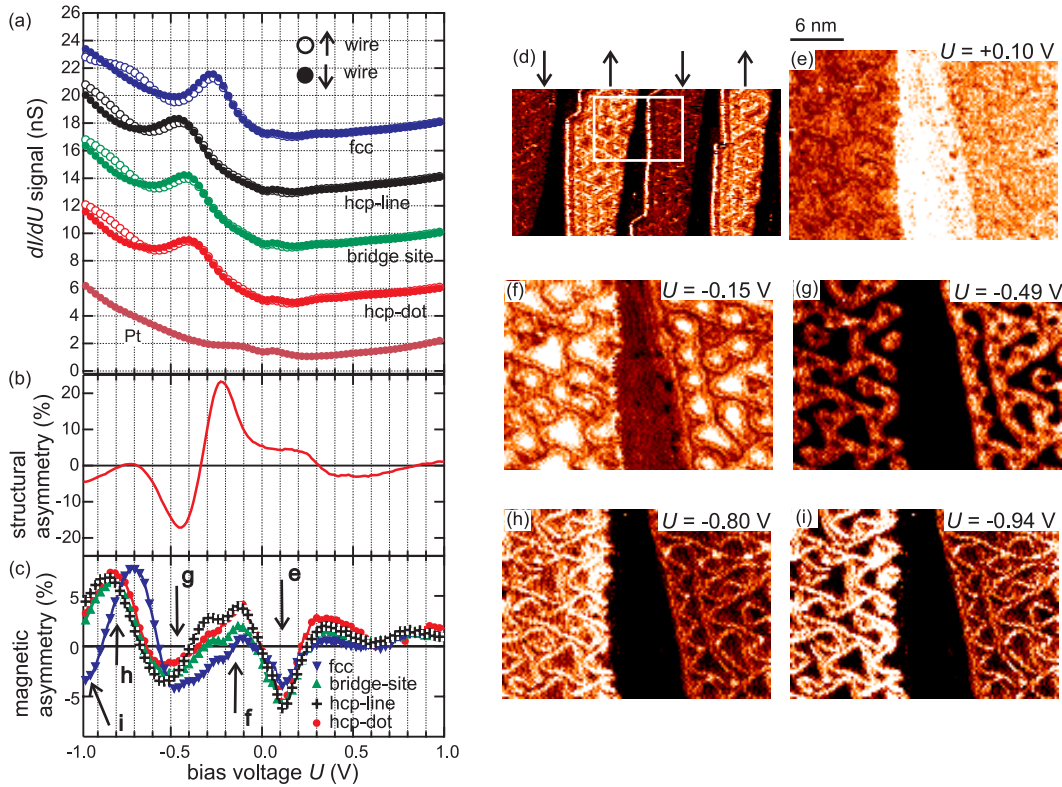


FIG. 2. (Color online) (a) Spin- and stacking-resolved dI/dU spectra on Co monolayer wires. Open and filled circles mark spectra taken on the upward and downward magnetized wire, respectively. The area of the spectroscopy measurement is indicated by the white rectangle in (d). For the stacking refer to Fig. 1(d). All Co spectra are offset by multiples of 4 nS. (b) Structural asymmetry between spin-averaged fcc and hcp-dot spectra. (c) Magnetic asymmetry between upward and downward Co monolayer wires for different stacking. (d) dI/dU map of alternatingly out-of-plane magnetized Co wires. (e)–(i) Selected spin-resolved dI/dU slices of the STS field. STS parameters: $I_{\text{stab}} = 1.5$ nA, $U_{\text{stab}} = +1.0$ V.

state they show different absolute dI/dU intensities compared to the stackings on the upper island.

These results motivate the performance of spatially resolved dI/dU spectroscopy. In order to get access to the spin- and energy-resolved electronic structure of the different stackings we performed spatially and spin-resolved STS which is shown in Fig. 2. The very high lateral resolution of the spectroscopic field enables us to assign the spectra taken above the Co monolayer atoms to a certain stacking sequence. Figure 2(d) shows a dI/dU map of alternatingly out-of-plane magnetized Co wires. The area where the spin-resolved dI/dU spectra were taken, is indicated by the white rectangle. Although the absolute orientation of the magnetization is unknown, we arbitrarily mark the wires by arrows and refer to upward and downward magnetized wires in the following. Figure 2(a) shows the dI/dU spectra obtained above the four different Co stackings on each wire and the spectrum above the bare Pt substrate (all obtained by averaging approximately 30 spectra). The Pt spectrum shows no outstanding spectroscopic features apart from a gently increasing dI/dU signal in the negative voltage range. All dI/dU spectra of the Co monolayer are also rather featureless in the positive voltage range. However, in contrast to the Pt spectrum they show a pronounced feature below E_F , with the peak energy depending on the specific stacking of the atoms. Independent of their magnetization direction, fcc-

stacked Co atoms of monolayer wires reveal a distinct peak located around -0.28 eV below E_F . Additionally, a small feature can be observed for the fcc spectrum obtained on the upward magnetized wire at -0.70 eV. In the spectra of the hcp- and bridgesite lines the characteristic peak is shifted to -0.48 and -0.42 eV, respectively, while the peak of the hcp-dot is located at -0.40 eV. In addition to variations originating from different stackings we observe a different intensity of this dominant peak due to the different magnetization directions, i.e., between the upward and downward magnetized wire. While these are generally small in the positive voltage range, we observe larger deviations close to the characteristic peak and in the energy range toward more negative bias voltages for all four different stackings.

In order to distinguish the spectroscopic differences due to a different stacking from those due to different magnetization, we calculate the structural asymmetry A_{struc} and the magnetic asymmetry A_{magn} of the spectra. The structural asymmetry is defined by

$$A_{\text{struc}} = \frac{dI/dU_{\text{fcc}} - dI/dU_{\text{hcp}}}{dI/dU_{\text{fcc}} + dI/dU_{\text{hcp}}} \quad (1)$$

with dI/dU_{fcc} and dI/dU_{hcp} representing the calculated spin-averaged spectra of fcc and hcp regions, respectively. The magnetic asymmetry is defined by

$$A_{\text{magn}} = \frac{dI/dU_{\uparrow} - dI/dU_{\downarrow}}{dI/dU_{\uparrow} + dI/dU_{\downarrow}} \quad (2)$$

with dI/dU_{\uparrow} and dI/dU_{\downarrow} representing the spin-resolved dI/dU spectra of the upward and downward magnetized wire for each stacking, respectively. Figure 2(b) shows exemplarily the structural asymmetry between the fcc and hcp-dot regions which confirms the impression that significant differences in dI/dU are located below E_F while the electronic structure in the positive voltage range is mostly stacking independent. The highest asymmetry values of around 20% are observed close to the energetic positions of the dominant peaks of the fcc and hcp-dot spectra. The magnetic asymmetries for each stacking are shown in Fig. 2(c). In the negative voltage range the magnetic asymmetries for the Co monolayer are higher than in the positive voltage range. They show distinct minima at about -0.50 eV and larger maxima around -0.80 eV. It appears as if the fcc asymmetry is compressed toward E_F compared to the other asymmetries. This is evident by a shift of the minimum and the maximum in the fcc magnetic asymmetry toward E_F by about 0.1 eV relative to the hcp asymmetries. This shift in asymmetry goes along with the corresponding stacking related shift of the main peaks observed in the dI/dU spectra for the fcc areas toward E_F . As a result the sign of the magnetic asymmetry is reversed for fcc regions compared to the other stackings below -0.9 eV. It is worth to mention that although the spin polarization of the tip states also influences the measured spin polarization, a different sign of the magnetic asymmetry at the *same* energy leads to the conclusion that the sample spin polarization is indeed inverted for fcc stacking relative to hcp stacking at energies between -1.0 eV and -0.9 eV.

In order to visualize the interplay between structural and magnetic asymmetry we display dI/dU slices at selected energies in Figs. 2(e)–2(i), the corresponding voltages are indicated in Fig. 2(c). The first slice in Fig. 2(e), which is taken in the positive voltage range at $+0.10$ eV, shows only a very weak influence of the stacking in accordance with the small structural asymmetry [cf. Fig. 2(b)]. In contrast, as a consequence of the different magnetic orientation of the wires, the dI/dU signal shows a difference between the upward and the downward magnetized wire. Figures 2(f) and 2(g) show slices at -0.15 eV and at -0.49 eV, respectively, where the structural asymmetry is strongest. While at -0.15 eV the fcc areas exhibit the highest dI/dU intensity, the bridgesites and hcp-lines show the highest intensity at -0.49 eV. This is in agreement with the inverted structural asymmetry between -0.20 and -0.50 eV as plotted in (b). The different magnetization of the wires is only slightly visible at these energies. Figures 2(h) and 2(i) finally display slices at -0.80 and -0.94 eV, respectively. At -0.80 eV the intensity of each stacking of the upward magnetized wire is higher than that on the downward magnetized wire. This is not the case at -0.94 eV, where the bridgesite lines exhibit a higher intensity on the upward than on the downward magnetized wire, while the fcc areas have a lower intensity on the upward than on the downward magnetized wire. This peculiar contrast reversal visualizes the already mentioned inversion of the

sample spin polarization for fcc areas with respect to the other stackings at about -0.90 eV.

Up to this point we can conclude that the electronic structure of the Co monolayer on Pt(111) changes significantly between the areas of the four different atom positions on a length scale of only a few atoms. The main change in the electronic structure is a shift of the dominating peak in the negative voltage range, which appears at -0.28 eV on the fcc areas and is shifted to lower energies for the other three stackings. Despite this strong heterogeneous electronic structure it is possible to deduce the magnetic orientation of the Co monolayer using the magnetic asymmetry of the spin-resolved dI/dU spectra.

2. Theoretical results

In order to understand the origin of the spectroscopic difference between fcc and hcp stacking of the Co monolayer on Pt(111), we have performed first-principles calculations using the full-potential linearized augmented plane wave (FLAPW) method in film geometry as implemented in the FLEUR code.²⁶ The system has been modeled by a symmetric 13-layer Pt slab with the experimental Pt in-plane lattice constant of 2.775 Å and an additional Co layer on both sides. We have applied the generalized gradient approximation of Perdew, Burke, and Ernzerhof.²⁷ Self-consistency for the charge density has been obtained with about 100 basis functions per atom and 44 \mathbf{k}_{\parallel} points in the irreducible wedge of the two-dimensional Brillouin zone (I2BZ). 81 \mathbf{k}_{\parallel} points in the I2BZ have been used for the calculation of the density of states (DOS).

The surface relaxation for the pseudomorphic Co layer in both fcc and hcp stacking has been carried out by force minimization. We obtained an equilibrium Co-Pt interlayer distance of 2.053 Å for hcp and 2.038 Å for fcc stacking, corresponding to an inward relaxation of 9.4% and 10.1%, respectively, compared to the bulk Pt interlayer distance. The fcc stacking of the Co layer is energetically more favorable by 67.4 meV/Co-atom than the hcp stacking. The magnetic moment of the Co atom was found to be $2.07 \mu_B$ and $2.10 \mu_B$ for fcc and hcp, respectively.

We applied the Tersoff-Hamann model to simulate the spectroscopic measurements. The differential conductance dI/dU is then proportional to the sample DOS in the vacuum at the position of the tip apex.²¹ The results for the majority and minority spin channels as well as the sum of both are presented in Fig. 3(a) for a tip-sample distance of 6.7 Å. The vacuum DOS in the energy range around the Fermi level is dominated by spin-minority states. The main minority peaks are found at $\varepsilon_{\text{fcc}} = -0.175$ eV and $\varepsilon_{\text{hcp}} = -0.250$ eV for the fcc and hcp structure, respectively, corresponding to a shift of $\Delta\varepsilon = 0.075$ eV.

In order to unambiguously pinpoint the electronic states contributing to the spectroscopic features, which the analysis of the band structure alone is not sufficient to provide, we have decomposed the vacuum DOS $n^{\downarrow}(\varepsilon)$ as a function of the in-plane k vector \mathbf{k}_{\parallel} : $n^{\downarrow}(\varepsilon, \mathbf{k}_{\parallel})$. We focus on the energies corresponding to the main peaks of the vacuum DOS for the minority spin in the two stackings, i.e., ε_{fcc} and ε_{hcp} [indicated by the dash-dotted lines in Fig. 3(a)]. The results are

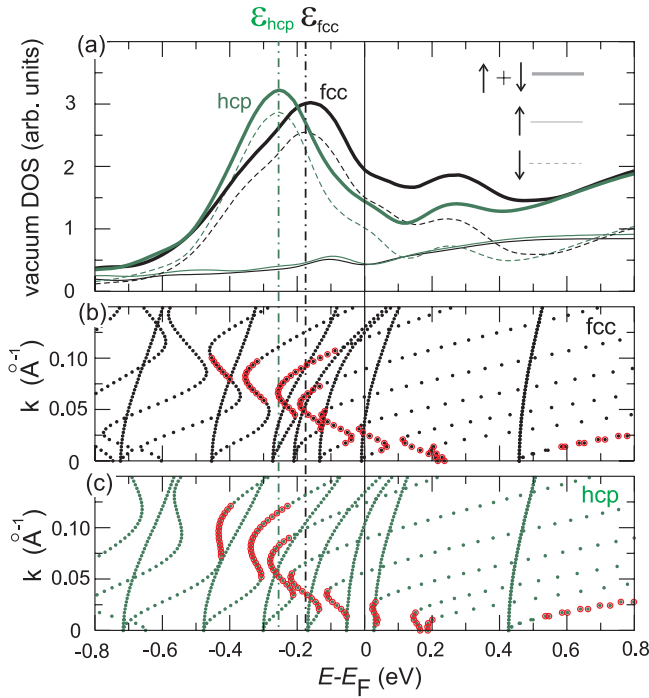


FIG. 3. (Color online) (a) Vacuum DOS for fcc (black) and hcp (green (gray)) stacking of 1 ML Co on Pt(111) at a distance of 6.7 \AA from the surface. The spin-majority (thin solid line), spin-minority (thin dashed line) contribution and the sum of both (thick solid line) are shown. The minority electron band structure along the $\bar{\Gamma}-\bar{M}$ line is plotted for the fcc (b) and hcp (c) stacking near the $\bar{\Gamma}$ point. States with a localization of more than 5% in the vacuum are marked in red (thicker dots).

shown in Fig. 4, where $n^\perp(\epsilon, \mathbf{k}_\parallel)$ has been plotted only in the vicinity of $\bar{\Gamma}$, as sketched in the inset, because of the \mathbf{k}_\parallel -dependent exponential decay of the electronic states in the vacuum. At ϵ_{hcp} , we observe in Figs. 4(a) and 4(b) for both fcc and hcp that the main contribution to the DOS comes from a hexagonal distribution of states in the BZ centered around the $\bar{\Gamma}$ point. $n^\perp(\epsilon, \mathbf{k}_\parallel)$ has a similar shape in the two stackings, suggesting that it originates from the same band. Information about the \mathbf{k}_\parallel of the states which are affected by a change in the stacking can be inferred from the difference of the vacuum DOS for the two structures. As can be seen in Fig. 4(c) these states are located along the $\bar{\Gamma}-\bar{M}$ high-symmetry lines.

Let us now focus on the fcc case only and analyze the vacuum DOS at different energies. A comparison of $n^\perp(\epsilon_{\text{hcp}}, \mathbf{k}_\parallel)$ in 4(a) to $n^\perp(\epsilon_{\text{fcc}}, \mathbf{k}_\parallel)$ in 4(d) reveals that for this stacking the \mathbf{k}_\parallel distribution of the vacuum DOS depends only weakly on energy. The width of the hexagonal distribution gets smaller as the energy increases, implying a negative effective mass for the involved band. For the hcp case a different trend is found. Interestingly, the DOS peaks for this stacking are located along the $\bar{\Gamma}-\bar{K}$ lines at ϵ_{fcc} (e), i.e., the hexagonal distribution appears 30° rotated compared to what was found for ϵ_{hcp} (b). Nevertheless, the difference in the vacuum DOS for fcc and hcp at ϵ_{fcc} [Fig. 4(f)] reveals that the spectroscopic contrast originates mainly from states

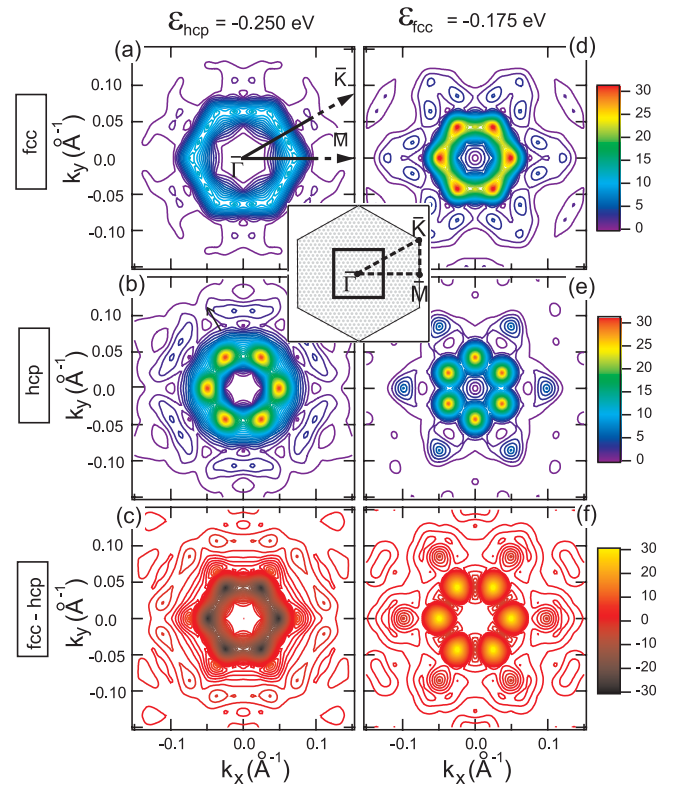


FIG. 4. (Color online) Decomposition of the vacuum DOS $n^\perp(\epsilon, \mathbf{k}_\parallel)$ in k space for fcc (a), (d) and hcp (b), (e) stacking of 1 ML Co on Pt(111) at energies of peak positions and the difference of them (c), (f). A sketch of the BZ and of the plotted area is depicted in the inset by the black square. 817 \mathbf{k}_\parallel points in the full BZ have been used for these plots. A Gaussian broadening of the levels of 20 meV has been included.

along the $\bar{\Gamma}-\bar{M}$ direction, similarly to what was found for ϵ_{hcp} .

The presented analysis of $n^\perp(\epsilon, \mathbf{k}_\parallel)$ tells us that further information can be extracted from the band structure along the $\bar{\Gamma}-\bar{M}$ direction, shown in Figs. 3(b) and 3(c). The states which are marked in red (thicker dots) are those with a high localization in the vacuum, thus giving the largest contribution to the vacuum DOS. Based on the strong resemblance to the Co(0001) electronic structure, where a very similar band stretches from -0.3 to $+0.1$ eV (Ref. 17), we can assert that these states describe a Co surface resonance. Our analysis of the charge distribution reveals that the character of this band changes from the band maximum at $\bar{\Gamma}$, where it is predominantly of p character, to the band minimum, where it is of d character with a small contribution of s and p states. In contrast to Co(0001), in the case of 1 ML Co/Pt(111) the surface resonance hybridizes with delocalized sp states which show a parabolic dispersion. As a result, gaps open in the surface resonance, which splits into several parts. Between -0.50 eV and $+0.2$ eV, the sp bands are slightly different for fcc and hcp stacking, due to the different coupling of the Co layer to the bulk Pt. This is clearly seen in the band structure, where the highly dispersive bands are located at different energies (e.g., compare the band energy at the $\bar{\Gamma}$ point). This

results in a different interaction between the surface resonance and the substrate for fcc and hcp stackings. As a consequence, the energy at which the hybridization gaps open as well as the gap size and the surface resonance dispersion are different for the two cases. The influence of the stacking fault on the band energy can be seen also in the flat bands which can be attributed to Co d states from charge distribution analysis.

It is worth noticing that the modification in the electronic structure due to the stacking fault is not simply a rigid energy shift, but it is state dependent and cannot be merely ascribed to a single state. The spectroscopic shift of 0.075 eV is an overall effect due to many states and this is also reflected by the large peak width. The peak of the vacuum DOS is located at the energy corresponding to the highest band density for each stacking. If we focus on an energy interval, e.g., 0.10 eV, centered at the position of the main peak of the hcp spectrum (ϵ_{hcp}), we can observe that in the hcp case there are three bands contributing to the vacuum DOS, in contrast to the fcc case, where only one band is present. On the other hand, around ϵ_{fcc} we find more bands contributing to the fcc vacuum DOS than to the hcp one.

In summary, the spectroscopic shift of 0.075 eV is due to the different coupling of the Co layer to the Pt substrate for the fcc and hcp stacking, resulting in different hybridization of the Co surface resonance with Co-Pt sp states. The widespread assumption that the main peaks in scanning tunneling spectra are related to states at the $\bar{\Gamma}$ point, due to their weak decay in the vacuum, is not valid here. As demonstrated for the Co/Pt(111) system the electronic structure in the close vicinity of $\bar{\Gamma}$, but not exactly $\bar{\Gamma}$, can be crucial for the spectral shape, depending on the character, dispersion, and energy of the states. Only the analysis of $n^{\downarrow}(\epsilon, \mathbf{k}_{\parallel})$ together with the band structure as described above allows us to unambiguously correlate specific spectroscopic features and electronic states.

3. Discussion

A comparison of the experimental and theoretical results reveals a good qualitative agreement. Both show a dominant feature in the negative bias regime with a comparable negative energy shift from fcc to hcp. The calculated peak positions are slightly closer to E_F . We ascribe this discrepancy to the reconstruction due to strain relief of the Co monolayer which is not included in the pseudomorphic slab assumed in the calculation. Thus, we can assign the dominant peak to a minority spin surface resonance below E_F . The calculations made it obvious that the different hybridization of this resonance with Co-Pt sp states is responsible for the observed differences in dI/dU at negative bias voltages. Such a stacking-dependent electronic contrast has been found for other Co systems like islands on Cu(111) and films on W(110).^{5,13,16,17} In contrast to our study these previous results were obtained on extended areas of different stacking in comparison to another extended area showing a different stacking. This is obviously different for the Co monolayer on Pt(111) where fcc, bridge, and hcp sites alternate on a lateral scale of only a few atoms. Nevertheless, the electronic struc-

ture of these few atoms wide areas is already well described by the infinite layer of the same stacking as shown by the calculations. This indicates that the position with respect to the underlying substrate, i.e., the stacking, is more important than the position of the neighboring Co atoms.

B. Response of Co monolayer and double-layer nanostructures to an external magnetic field

In order to study the magnetic properties of the Co monolayer as well as the Co double-layer nanostructures and to verify the magnetic origin of the observed contrasts in dI/dU maps we probed the Co structures in variable magnetic fields, which were applied along the surface normal.

1. Co monolayer nanostructures

Figures 5(a)–5(d) show selected out-of-plane sensitive magnetic dI/dU maps with an applied external magnetic field B as indicated. The sample preparation, which has been described in Sec. II, results in some free-standing Co islands and Co wires which are attached to the Pt step edges. While the Pt substrate has a uniform dI/dU signal with low intensity, a two stage magnetic contrast of the oppositely out-of-plane magnetized Co is clearly visible for the islands as well as the wires. Figure 5(a) displays the magnetic virgin state of the sample at 0 T and the amount of both opposite magnetization directions of the Co structures is approximately equal. After increasing the magnetic field to +0.3 T (b), some Co areas which are marked in the dI/dU map changed their magnetic orientation. From this contrast reversal we can directly conclude that these bright areas are now aligned with the direction of the external field. For the left marked wire in (b), it can be observed that the field-induced reorientation process does not change the magnetization of the wire completely, but only part of the wire switched the magnetization due to a constriction or gap. At a magnetic field of +0.8 T all Co structures appear bright except one comparably large Co island marked in Fig. 5(c). Figure 5(d) displays the magnetic state at remanence. A direct comparison to the previous dI/dU map in (c) shows that all wires and islands remain in their magnetic state.

Analyzing the magnetic state of the Co nanostructures and plotting the percentage of the bright Co areas at several applied magnetic fields leads to a hysteresis curve, which is displayed in Fig. 5(e). Since the external magnetic field is applied along the easy anisotropy axis, the hysteresis curve shows a typical ferromagnetic shape with a very high remaining magnetization after field removal. The extracted coercivity of this area of the monolayer Co sample is about $\mu_0 H_c = 0.25 \pm 0.05$ T. This value is comparable to the coercivity observed for spatially averaging experiments on few atom wide Co wires on Pt(111) at low temperatures.⁸ As visible in (e) the obtained hysteresis curve does not show a simple square loop shape but is slightly canted. This can be understood by taking into account that the magnetic reorientation process occurs not at the same magnetic field for each Co structure, but progresses successively.²⁸ In general we observe that larger islands as well as wider wires seem to switch abruptly from one saturated state to the opposite one

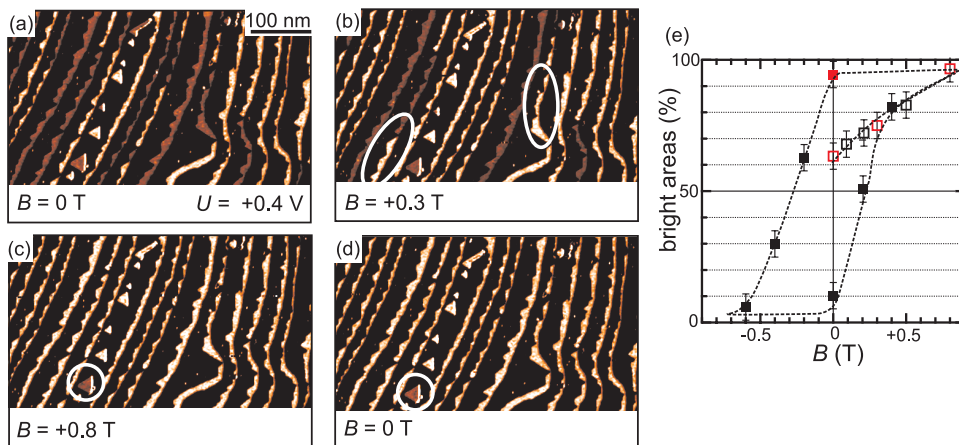


FIG. 5. (Color online) (a)–(d) Selection of out-of-plane sensitive magnetic dI/dU maps of Co monolayer wires and islands in the presence of an external magnetic field applied perpendicular to the surface plane. The bright or dark appearance of the Co corresponds to a parallel or antiparallel alignment of the tip and sample magnetization. (e) Hysteresis loop obtained by plotting the percentage of bright domains at certain magnetic fields. The open squares belong to the initial magnetization curve and the red color (gray) indicates the dI/dU maps shown. The dashed line is a guide to the eye.

at higher applied magnetic fields than smaller Co structures. Furthermore, the reorientation process itself is different for wires and islands. While the Co islands are always in a single domain state on the time scale of this measurement, wires with a sufficient width are reoriented by domain wall movement.

The existence of these domain walls allows the critical examination of recent results obtained on nanoscale Co monolayer islands. Namely, Rusponi *et al.*³ interpreted their MOKE and STM measurements in terms of strongly coordination-dependent magnetic anisotropies: while—according to Ref. 3—Co atoms at the island perimeter exhibit a very high out-of-plane anisotropy of 0.9 ± 0.1 meV per atom a weak in-plane anisotropy ($E_A = -0.03 \pm 0.01$ meV per atom) is found for surface atoms within the islands. Such magnetic properties have two significant consequences on the nanoscale domain structure of sufficiently large islands and wires: first, the easy axis shall rotate from out-of-plane to in-plane if the lateral dimensions exceed the magnetic correlation or exchange length. Second, the strongly enhanced anisotropy at Co step edges should lead to very narrow domain walls. While we cannot scrutinize the latter hypothesis due to the complex structural and electronic properties of the Co monolayer dislocation network on Pt(111) (cf. Fig. 1), we were able to investigate whether the easy axis of magnetization changes with increasing distance from the Co step edge by analyzing domain walls in Co nanowires. As shown in Fig. 5, however, domain walls are preferentially located at constrictions which are few nanometers wide only, if the terraces are particularly narrow. Therefore, we have studied Co nanowires which were grown on much wider Pt(111) terraces and exhibit a width of 15–25 nm as shown in the dI/dU map of Fig. 6(a). In the central part of the image a dark domain can be recognized which is surrounded by two bright domains. Both domain walls separating the three domains are located in constrictions and are about 20 nm long. Since these data were measured with an out-of-plane sensitive probe tip we can con-

clude that the Co nanowire is perpendicularly magnetized even 20 nm away from the Co step edge. But how does this distance relate to the magnetic exchange length? This can be

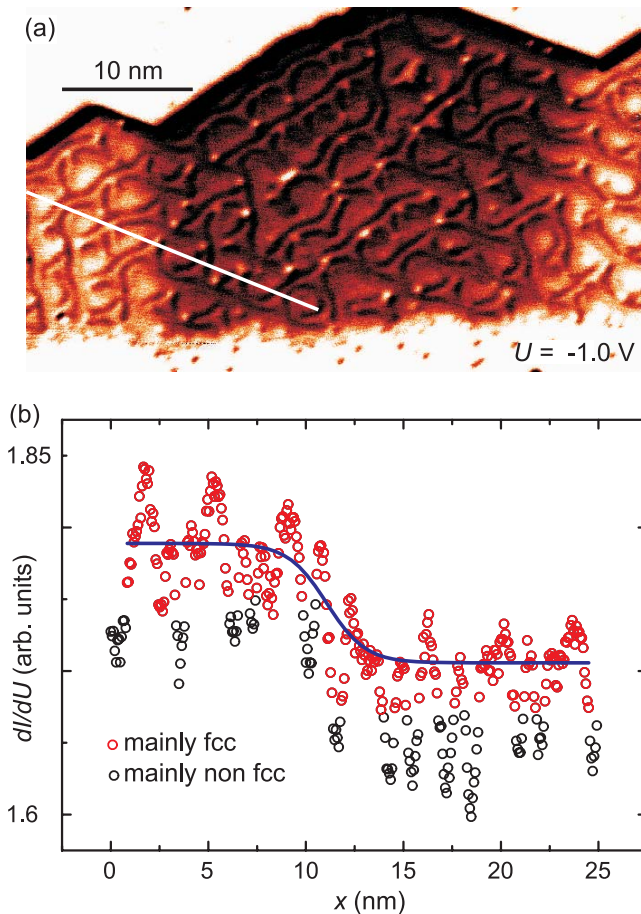


FIG. 6. (Color online) (a) Out-of-plane sensitive magnetic dI/dU map of a Co monolayer wire with three domains. (b) Domain wall profile (open circles) along the line marked in (a). The solid line gives a fit to the red (gray) data points.

analyzed by a closer inspection of the domain wall profile. For this purpose we have taken a profile of the dI/dU signal along the white line in Fig. 6(a). The result is plotted in Fig. 6(b). In order to minimize the influence of the inhomogeneous spin-averaged electronic structure due to different stacking (see Sec. III A) we have not taken the line section perpendicular to the domain wall but under an angle of 60° . Thereby, mostly fcc sites are crossed and hcp sites are avoided as far as possible. The line section shows two levels of dI/dU signal strength on the left and the right side which represent the oppositely magnetized domains and the transition area in between. While the data points on each domain oscillate due to the remaining stacking influence, the signal becomes much smoother when neglecting the data points originating from the hcp-lines which are given in black color. The remaining red (gray) data points are fitted with a standard domain wall function (Ref. 23)

$$y = y_0 + y_{\text{sp}} \tanh\left(\frac{2(x-x_0)}{w}\right) \quad (3)$$

which is based on continuum micromagnetic theory.²⁹ y_0 and y_{sp} are the spin-averaged and the spin-polarized part of the dI/dU signal, x_0 is the position of the domain wall center, and w represents the domain wall width, which is determined by the exchange stiffness A and the effective anisotropy constant K_{eff} by

$$w = 2 \sqrt{\frac{A}{K_{\text{eff}}}}. \quad (4)$$

As shown by a solid line in (b) the best fit is obtained for a domain wall width of approximately 4 nm, i.e., much narrower than the structural width of the Co nanowire. This observation indicates that the intrinsic anisotropy of surface coordinated Co atoms on Pt(111) is not in-plane as proposed by Rusponi *et al.*³ but out-of-plane instead. This conclusion is also consistent with our observation that the magnetization of triangular Co monolayer islands is homogeneous across the islands' surfaces even though the base length of some islands is about thirty times larger than the exchange length $L=w/2$ extracted from Fig. 6(b). Assuming a reasonable value for A ,³⁰ the anisotropy constant results in $+0.08 \text{ meV/atom} \leq K_{\text{eff}} \leq +0.17 \text{ meV/atom}$.

2. Co double-layer nanostructures

Figures 7(a)–7(d) display out-of-plane sensitive magnetic dI/dU maps of Co double-layer nanostructures (0.6 AL) measured at different magnetic fields. The sample preparation is described in Sec. II. In addition to free standing double-layer islands, some double-layer structures are attached to the Pt step edges. Again we observe a homogeneous electronic structure for the Pt(111) surface and a two-stage contrast for the Co double-layer islands. This shows that the double-layer Co islands are ferromagnetic with an out-of-plane anisotropy and thus are magnetized either up or down with respect to the surface plane, in accordance with the observations reported in the literature.^{3,9} An increase from 0 T (not shown) to +2.0 T in Fig. 7(a) still does not reveal any switching of the Co double-layer magnetization

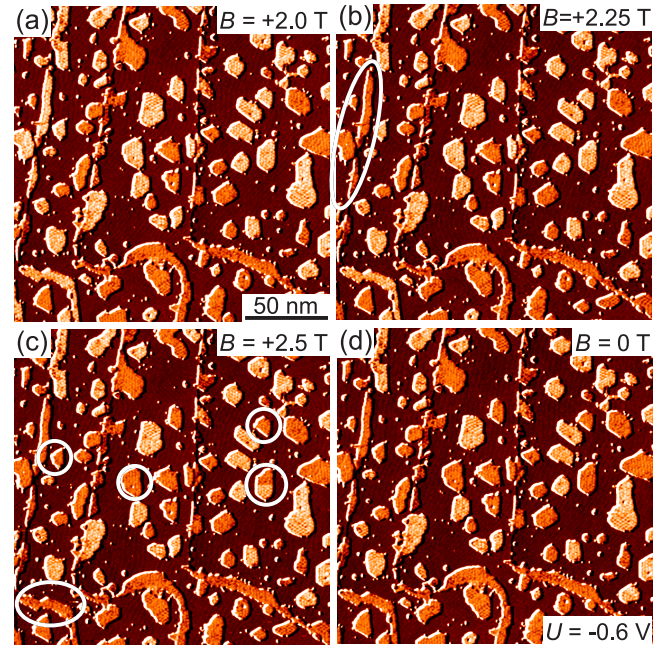


FIG. 7. (Color online) (a)–(d) Selection of out-of-plane sensitive magnetic dI/dU maps of compact Co double-layer islands in the presence of an external magnetic field applied along the surface normal. The bright or more dark appearance of the Co corresponds to a parallel or antiparallel alignment of the tip and sample magnetization.

and thus Fig. 7(a) shows the magnetic virgin state. Both magnetic orientations are distributed equally. First changes of the magnetic state are observed at an applied field of +2.25 T in (b). The magnetization of some structures is rotated as indicated. It is observed that the switched structures are directly attached to the Pt step edge. Also some free standing Co islands switched at a field of +2.5 T shown in (c). This is the maximum available external field which surprisingly is not sufficient to align the magnetization of all islands. While every island shows a uniform magnetization, i.e., it is in a single domain state, on top of one island marked in (c) both opposite magnetization directions are visible. This is caused by a magnetization reversal of the island in between two subsequent lines of the image while passing the island. After the removal of the external field shown in Fig. 7(d), a comparison to (c) reveals a 100% remanence, i.e., all Co islands remain in their previous magnetic state. Since an influence of the external magnetic field on the sample was first detected between +2.0 T and +2.25 T we can conclude that $\mu_0 H_c > 2.0 \text{ T}$. The result suggests a high out-of-plane anisotropy of the islands. The surprisingly high coercivity is to our knowledge higher than all previously reported coercivities for Co structures on Pt(111). While it is already known that Co double-layer islands on Cu(111) exhibit a high coercivity between 1.0–1.5 T (Ref. 5), the values of the present Co double-layer islands studied in this work are even higher. This again emphasizes the important role the substrate plays for the magnetic properties of nanoscale structures.

IV. SUMMARY

In summary we have presented a detailed study of the structural, electronic, and magnetic properties of monolayer Co islands and wires on Pt(111). Although the Co monolayer is electronically highly heterogeneous due to a lattice mismatch induced dislocation network, it is possible to observe the out-of-plane magnetized domains by spin-resolved STS. Independent of the magnetization direction the spin-resolved spectra exhibit a dominant peak at about -0.28 eV for fcc, which is shifted downward by more than 0.12 eV for hcp- and bridgesite stacked regions, which are only several atoms wide. Accordingly the peaks in the magnetic asymmetry in this energy range are also shifted downward on the hcp- and bridgesite regions relative to the fcc regions.

In order to understand the spectroscopic stacking dependency, first-principles calculations for pseudomorphic Co monolayers on Pt(111) in fcc- and hcp-stacking were performed. A detailed analysis revealed that the dominant peak originates from a d -like Co surface resonance of minority-spin character which is similar to the state found for thicker Co(0001) films on different substrates.¹⁷ The spectroscopic shift between differently stacked areas results from different hybridization of the Co surface resonance with Co-Pt sp states. Even though the calculation was done for infinite areas of a given stacking it reproduces the experimental observations fairly well where the same stacking is only present for a few atoms.

We find an out-of-plane magnetization of the Co monolayer wires and islands. By measuring the domain wall width on wires, the magnetic exchange length is determined to be less than 2 nm. According to Ref. 3 the magnetic anisotropy of the surface atoms within the islands is weakly in plane and only the perimeter atoms exhibit a large out-of-plane anisotropy. We have no experimental indications to support this: islands with a base length as large as thirty times the exchange length still show a homogeneous out-of-plane magnetization. In order to reproduce the measured domain wall width we propose an out-of-plane anisotropy of $+0.08$ meV/atom $\leq K_{\text{eff}} \leq +0.17$ meV/atom for atoms within the island.

Finally, our measurements in the presence of an external magnetic field show that the coercivity of Co nanostructures is highly increased by a change of sample morphology. While the Co monolayer system exhibited a coercivity of $\mu_0 H_c = 0.25 \pm 0.05$ T, the Co double-layer nanostructures show a surprisingly high coercivity of $\mu_0 H_c > 2.0$ T.

ACKNOWLEDGMENTS

We thank A. Kubetzka, O. Pietzsch, and E. Y. Vedmedenko for fruitful discussions. Financial support from the “Deutsche Forschungsgemeinschaft” (SFB 668), from the “Stifterverband für die Deutsche Wissenschaft,” and from the Interdisciplinary Nanoscience Center Hamburg is gratefully acknowledged.

*Corresponding author. Email address: fmeier@physnet.uni-hamburg.de

¹P. Gambardella, A. Dallmeyer, K. Maiti, M. Malagoli, W. Eberhardt, K. Kern, and C. Carbone, *Nature (London)* **416**, 301 (2002).

²P. Gambardella, S. Rusponi, M. Veronese, S. Dhési, C. Grazioli, A. Dallmeyer, I. Cabria, R. Zeller, P. Dederichs, and K. Kern, *Science* **300**, 1130 (2003).

³S. Rusponi, T. Cren, N. Weiss, M. Epple, P. Bulushek, L. Claude, and H. Brune, *Nat. Mater.* **2**, 546 (2003).

⁴L. Diekhöner, M. A. Schneider, A. N. Baranov, V. S. Stepanyuk, P. Bruno, and K. Kern, *Phys. Rev. Lett.* **90**, 236801 (2003).

⁵O. Pietzsch, A. Kubetzka, M. Bode, and R. Wiesendanger, *Phys. Rev. Lett.* **92**, 057202 (2004).

⁶L. Niebergall, V. S. Stepanyuk, J. Berakdar, and P. Bruno, *Phys. Rev. Lett.* **96**, 127204 (2006).

⁷O. Pietzsch, S. Okatov, A. Kubetzka, M. Bode, S. Heinze, A. Lichtenstein, and R. Wiesendanger, *Phys. Rev. Lett.* **96**, 237203 (2006).

⁸P. Gambardella, A. Dallmeyer, K. Maiti, M. C. Malagoli, S. Rusponi, P. Ohresser, W. Eberhardt, C. Carbone, and K. Kern, *Phys. Rev. Lett.* **93**, 077203 (2004).

⁹S. Rusponi, N. Weiss, T. Cren, M. Epple, and H. Brune, *Appl. Phys. Lett.* **87**, 162514 (2005).

¹⁰P. Grütter and U. T. Dürig, *Phys. Rev. B* **49**, 2021 (1994).

¹¹E. Lundgren, B. Stanka, M. Schmid, and P. Varga, *Phys. Rev. B* **62**, 2843 (2000).

¹²Y. Yayon, X. Lu, and M. F. Crommie, *Phys. Rev. B* **73**, 155401 (2006).

¹³A. L. Vázquez de Parga, F. J. Garcíá-Vidal, and R. Miranda, *Phys. Rev. Lett.* **85**, 4365 (2000).

¹⁴S. N. Okuno, T. Kishi, and K. Tanaka, *Phys. Rev. Lett.* **88**, 066803 (2002).

¹⁵M. Prutzer and H. Elmers, *Surf. Sci.* **550**, 223 (2004).

¹⁶M. Prutzer and H. J. Elmers, *Phys. Rev. B* **72**, 035460 (2005).

¹⁷J. Wiebe, L. Sacharow, A. Wachowiak, G. Bihlmayer, S. Heinze, S. Blügel, M. Morgenstern, and R. Wiesendanger, *Phys. Rev. B* **70**, 035404 (2004).

¹⁸M. Bode and R. Wiesendanger, in *Magnetic Microscopy of Nanostructures*, edited by H. Hopster and H. P. Oepen (Springer, Berlin, 2006).

¹⁹This sketch is inspired by Ref. 11.

²⁰O. Pietzsch, A. Kubetzka, D. Haude, M. Bode, and R. Wiesendanger, *Rev. Sci. Instrum.* **71**, 424 (2000).

²¹J. Tersoff and D. R. Hamann, *Phys. Rev. Lett.* **50**, 1998 (1983).

²²M. Bode, *Rep. Prog. Phys.* **66**, 523 (2003).

²³A. Kubetzka, M. Bode, O. Pietzsch, and R. Wiesendanger, *Phys. Rev. Lett.* **88**, 057201 (2002).

²⁴E. Lundgren, B. Stanka, W. Koprolin, M. Schmid, and P. Varga, *Surf. Sci.* **423**, 357 (1999).

²⁵C. Shern, J. Tsay, H. Her, Y. Wu, and R. Chen, *Surf. Sci.* **429**, L497 (1999).

²⁶<http://www.flapw.de>

²⁷Y. Zhang and W. Yang, *Phys. Rev. Lett.* **80**, 890 (1998).

- ²⁸O. Pietzsch, A. Kubetzka, M. Bode, and R. Wiesendanger, *Science* **292**, 2053 (2001).
- ²⁹A. Hubert and R. Schäfer, *Magnetic Domains* (Springer, Berlin, 1998).
- ³⁰In order to obtain an appropriate value of the exchange stiffness of the ML, A_{ML} has been estimated in two ways. Based on the information that 0.8 ML Co/Pt(111) is still ferromagnetic above room temperature (Ref. 25) and the assumption $T_C \propto A$, we ob-

tain $A_{\text{ML}} = 7.0 \times 10^{-12}$ J/m with $T_{\text{C,bulk}} \approx 1400$ K and $A_{\text{bulk}} = 3.0 \times 10^{-11}$ J/m. T_C is the Curie temperature. A second way to estimate A_{ML} is based on using $A \propto N$ where N is the coordination number of an atom. Since N is reduced from twelve for bulk atoms to six for a monolayer atom, A_{ML} is given by 1.5×10^{-11} J/m. Both values derived for A_{ML} provide a reasonable estimate for the correct value.